CHAPTER - 4

MEASUREMENT OF TOTAL CROSS SECTION AND EXTRACTION OF PAIR PRODUCTION CROSS SECTION FROM MEASURED TOTAL CROSS SECTION

4.1 INTRODUCTION

Photons interact in several ways with atomic electrons, nuclei or fields of nuclei and of electrons. In the low energy region ($E < 10$ Mev) the most important interactions are (i) incoherent scattering by atomic electrons, (ii) Coherent Rayleigh scattering by atomic electronx, (iii) Photoelectric absorption by atoms and (iv) electron positron pair production in the field of the nucleus.

The remaining interaction processes produce negligible effects in the present energy range(1.115 - 1.332 Mev).

Consequently the total photon interaction cross section per atom is given by the sum of the cross sections for the fundamental processes (i) to (iv) which depend on the photon energy and target Z.

A narrowly collimated beam of photon shows a truely exponential attenuation in matter under some experimental conditions. An exponential attenuation is due to the fact that photons are attenuated in the first collission (a single shot process). As a result, a measurement of transmission of a narrowly collimated beam

of photons through a slab of the absorber of known thickness enables the determination of the total scattering cross section.

From the theoretically known values of the other photon interaction cross sections pair production cross section can be evaluated.

4.2 EXPERIMENTAL CONDITIONS

The experimental conditions to impose are the following:

(a) All the photons which are singly scattered in the absorber even at very small angles and all other secondary photons created in the absorber must not reach the detector. In other words collimated photons which penetrate the absorber without interaction should reach the detector.

(b) Photons undergoing multiple scattering in the absorber must not affect the good geometry condition of the primary beam after transmission. Many of the previous experiments failed to satisfy this condition as is evident from the discrepancies between some of the experimental results (Co-70, Pa-68).

4.3 EXPERIMENTAL ARRANGEMENTS

The principle of transmission experiment under ideal condition is quite simple and straight forward. Deviations from ideal good geometry condition lead to uncertainty in the measurement. The multiple scattering in the absorber thickness also introduce error in the measurement.

4.3.1 Collimation of Gamma ray source and detector

The experimental set up (Fig. 4.1) has been arranged under rigorous collimation requirements to obtain good geometry conditions for the primary beam before and after transmission and to reduce background photons from materials other than the absorber slab.

The gamma ray source was within a 10 cm deep conical bore in a lead block. The minimum thickness of lead shielding at the side and the back of the source was 20 cm. The collimator number 1 is a 23 cm iron block having a collimating bore of exit aperture 0.4 cm diameter. The collimation of primary beam between absorber and detector was provided by collimator numbers 2-5 of total thickness of 60 cm of iron. The collimators shield prevent photons scattered in the shields and environs from reaching the detector. The collimators were mounted on rigid

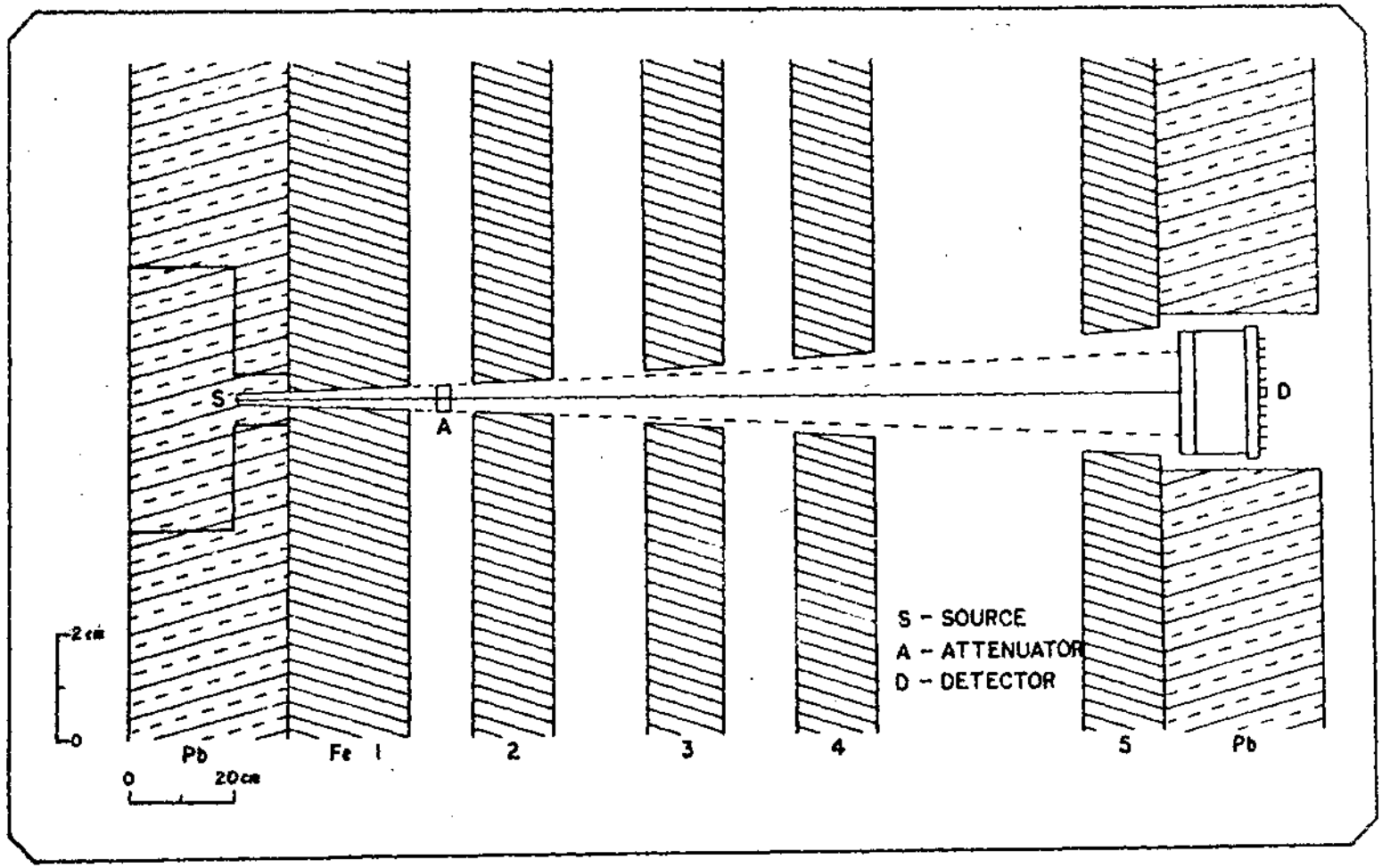
S
A
D
2 cm
0
Pb
Fe
1
2
3
4
5
Pb
0
20 cm
S - SOURCE
A - ATTENUATOR
D - DETECTOR

F I G. 4.1.

optical bench such that their positions could be adjusted to obtain different geometry.

Table - 4.1

BASIC DATA FOR THE NARROW BEAM GEOMETRY

Fig. 4.1

1. Source to detector distance - 175 cm
2. Source diameter - 0.3 cm
3. Detector diameter - 2.4 cm
4. Absorber diameter - 0.5 cm
5. Absorber to detector distance - 120 cm
6. Maximum scattering angle for the scattered photon - 23
7. Maximum solid angle of the scattering cone from observer to detector centre - 13.3×10^{-6} Sr

4.3.2 PRECAUTION AGAINST SMALL ANGLE SINGLE SCATTERING

As mentioned earlier the detector should respond only to primary photons that are transmitted by the absorber without any interaction, photons scattered coherently or incoherently at small angles cannot be

resolved out from the primary photons. Number of photons scattered at small angles and detected by the detector can be minimised by decreasing the solid angle of the collimating system between the absorber and detector. In the geometry of the present experiment no photon scattered at an angle greater than 23' could reach the detector.

4.3.3 Precaution against multiple scattering

Multiple scattering depends on the absorber thickness which becomes negligible if the absorber thickness is within two mean free paths (m.f.p= $1/\mu$) of primary photons. For measurement with each absorber the maximum thickness was determined in trial experimental runs under requirements that 'full width at half maximum' of photopeak is not changed when the absorber is placed in the path of the beam.

4.3.4 Requirements for the detector system

Even with high degree of collimation of the photon beam, adequate precaution must be taken to minimise the response of the detector to photons whose energy is smaller than primary photon energy using high energy resolution detector by setting the detector bias appropriately. The

The scintillation detector used is 1" x 1" NaI (Tl) crystal mounted on a RcA 6199 photo multiplier tube that was shielded by 2.5 cm Pb shield. Measured resolution at Co^{60}- 1.332 Mev is 8% for FWHM of the photopeak.

4.3.5 Gamma ray sources

The description of the sources used in the measurement is given in Table 4.2.

Table - 4.2

Source	Active size	Physical form	Half life	Strength in mci	Photon energy in Mev
Sc-46	4 mm dia x 3 mm long	Sealed source	84 days	130	.889 1.120
Zn-65	4 mm dia x 3 mm	Sealed source	245 days	140	1.115
Co-60	3 mm x 2 mm	Sealed source	5.3 years	100	1.173 1.332

4.3.6 Absorbers

Measurements were made an eight elements which were at least 99.9% pure. Out of these elements two were in elemental form remaining six were oxides. The powdered

oxides were kept inside a thin perspex tubes 1 cm in internal diameter. Extreme precaution was taken to ensure uniform packing of the powdered sample. Thickness was determined from measurement of its area and weight. The thickness was chosen in trial experiments to minimise multiple scattering.

4.2 Experimental procedure and measurements

When the attenuation of the photon beam in the absorber is exponential the total attenuation coefficient is given by the relation

$$I_x = I_0 e^{-\mu x} \qquad \ldots (4.1)$$

where I_0 is the beam intensity incident on the absorber slab, I(x) is the intensity of the transmitted beam and x is the sample thickness in gm/cm^2. In terms of the transmission ratio $R = \frac{I(x)}{I_0}$ and absorber thickness x, μ (cm^2/gm) is given by

$$\mu = \frac{\ln\left(\frac{1}{R}\right)}{x} \qquad \ldots (4.2)$$

Attenuation coefficient is related to the total photon cross section in cm^2/atom by

$$\mu = \sigma_t N/A \qquad \ldots (4.3)$$

where N is the Avagadro's number (6.022×10^{23} atom/gm-atom) and A is the atomic weight of the absorber material. So σ_t in barns per atom is given by

$$\sigma_t = \mu / \frac{N}{A} \times 10^{-24} \qquad \ldots (4.4)$$

The value of the factor $\frac{N}{A} \times 10^{-24}$ for absorbers studied is given in Table A in appendix.

Value of μ and hence σ_t can be determined from measurement of four quantities i.e. absorber thickness x, the incident beam intensity, transmitted beam intensity and the background. If the absorber is a chemical compound, unknown total attenuation coefficients of any constituent element can be evaluated from the measured attenuation coefficient of the compound and the known coefficient of the other constituent elements using the equation

$$\mu_{com} = \sum w_i \mu_i \qquad \ldots (4.5)$$

where w_i is the proportion by weight of the ith constituent and μ_i is the attenuation coefficient of the ith constituent.

If several transmission measurements are made for a given sample thickness at a particular gamma ray energy, the attenuation coefficient can be calculated using the mean value of R and the average sample thickness x. The standard deviation S of the measured value of μ in terms of standard deviation S_R of R and S_x of x is given by

$$S_\mu^2 = \left(\frac{\partial \mu}{\partial R}\right)^2 S_R^2 + \left(\frac{\partial \mu}{\partial x}\right)^2 S_x^2 \quad \ldots (4.6)$$

If for the same sample the measurement is repeated at more than one thickness at the same energy by maintaining the exponential attenuation condition a mean value of can be evaluated with standard deviation of the mean value given by

$$\overline{S}^2 = \frac{1}{n^2} \sum \overline{S_{\mu,i}^2} \quad \ldots (4.7)$$

where S is the standard deviation of obtained for the ith thickness of the sample.

4.2.1 Procedure

The detector system was first set for a primary photon energy. Bias levels were adjusted to record only the photopeak of the -ray spectra. These settings were recorded as a function of time to determine the long term stability of the electronics. It was found that the drift of the photopeak was less than 1 channel in 24 hours.

The system was calibrated for energy and recalibration once in a week was done during the whole course of measurement.

A holder was used to place the sample in position normal to the beam. The holder could be displaced laterally with respect to the incident beam, so that different parts of the sample area could be exposed to the incident beam. With the sample in position and a 20 cm lead stopper between collimater nos. 4 and 5 the mean background count rate was determined (i) when the source was not placed in its position and (ii) when the source was in position. Using the strongest source (Zn-65, 140 mci) variation in counts during 4 hours was 1.5% which demonstrate the

effectiveness of the shields and collimators in preventing any rise in background. Powdered sample count rate with empty holder was taken for the no absorber count to take into account the contribution of the container to any attenuation of the incident radiation. For each sample, counts for the same time was taken successively in the following sequence. Background counts without absorber, counts with absorber and so on. Counting time was adjusted from 30 minutes to hours to reduce the statistical error to .3%. In addition to statistical uncertainty, the systematic errors arising from geometry, target, source size and background scattering effects have been reduced to an extent less than the statistical errors.

4.4.2 Measurements

(i) Effect of geometry of the experimental set up on the measurements.

The effect of geometry on the measured total cross section was studied by changing the solid angle between the absorber and detector and found to have no significant influence on the results.

(ii) Effect of multiple scattering on the measurement.

Effect of multiple scatering on the measured total cross sections was studied.

The 'FWHM' increased slightly over that for the

incident spectrum if the absorber thickness exceeds a certain thickness x_m indicating the presence of multiply scattered photons in the attenuated beam. Care was taken to ensure that experimental thickness of the sample to be well below x_m.

(iii) Attenuation data

Total attenuation data was obtained from measurement made at a solid angle of 13.3×11^{-6} Sr between the absorber and the detector. The average sample thickness was determined to an accuracy of 0.05%.

Total cross section for M_f^o, La, Ce, Nd, Sm and Gd were evaluated from measured attenuation coefficient of the oxides of these elements and making use of equation (4.5) and table B in the appendix.

4.3 Evaluation of the uncertainty in the measurements

Errors in the measured attenuation coefficients are the combined standard deviation of the set of transmission ratios and the standard deviation of the set of measured thickness values. Transmission count at a number of positions over the area of each sample was taken to minimise the experimental error due to point to point variation of the sample thickness. The systematic errors arising from the following were taken into account.

(a) The detector detects some of the photons scattered at very small angles and other secondary radiations (bremsstrahlung, annihilation photons) introduced in the absorber.

In the present experimental arrangement contributions from single incoherent and coherent scattering are negligible and corrections to the data for small angle scattering are not necessary.

(b) The detector detects some of the multiply scattered photons from the absorber.

In the measurement with thick absorbers, some of the photons may suffer more than one interaction and may ultimately reach the detector. To minimise the effect, the narrowly collimated incident beam was made to intercept a small area of the absorber and making measurement on relatively their samples.

(c) The detector detects at the photopeak energy of one r-ray some other r-rays close in energy.

This is due to (8-10)% resolution near 1 Mev of NaI (Tl) detector system. For measurement with 1.173 and 1.332 Mev photons from Co-60 source and at 0.889 and 1.120 Mev from Sc-46 source some corrections to the data were determined experimentally by the following method

adopted by Colgate (Co-52). The FWHM of Co-1.173 Mev photopeak was determined to be 4 volts. The detector system with analyser window of 4 volts was set on the Zn-65 1.115 Mev (Energy being close to 1.173 Mev) and the mean counting rate determined. The analyser bias was then shifted to a higher level by an amount equal to the energy. 159 Mev between 1.332 and 1.173 Mev and the mean counting rate determined with same window. The second rate gives the number of 1.115 Mev photons counted at an energy difference of.159 Mev on the photopeak of 1.274 Mev. The ratio of the count rate of 1.274 Mev to that at 1.115 Mev was taken as the relative contribution of one photopeak to the other. Experimentally found value for this relative contribution was 2%. The procedure was repeated for Mn-54 (.840) for measurement with Sc-46 source. The relative contribution for two energies .889 and 1.120 Mev was 1%.

(d) Effect of energy degradation of primary photons due to Compton scattering in the source material.

Compton scattering of the primary photon in the source material changes the energy of the photons. The magnitude of the effect can be minimised by choosing small sources and narrowly collimating the source. The

effect was found to be small for the present measurements at very small angles with available sources to affect the data.

(e) The counting system losses some counts at high counting rate due to its finite resolving time.

The resolving time of the counting set up experimentally determined by standard method was 10 sec. The direct count rate varied from 25 per sec to 729 per sec. So the count loss was small and taken in to consideration in the analysis.

(f) The effect of Background scattering

As already mentioned in section 4.1 the actual background count rate during all the measurement was small. Transmitted and direct counts were corrected for background.

4.4 Evaluation of the cross section

Measured total cross section, λ^{s} using equation (4.1) and those obtained using equation (4.5) and the table A in the appendix are listed in table 4.3. Theoretical cross sections for the competing interactions i.e. photo-electric effect, total scattering cross section (coherent

Table - 4.3

MEASURED TOTAL CROSS SECTION

Element	Atomic number	Energy in Mev			
		1.115	1.120	1.173	1.332
Mo	42	8.7422 ±.0047	8.7281 ± .0047	8.5243 ± .0031	7.9788 ±.003
La	57	12.5072 ±.0069	12.4769 ± .0069	12.1629 ± .0046	11.5699 ± .0046
Ce	58	12.7839 ±.006	12.7531 ± .0069	12.4243 ± .0046	11.6100 ± .00465
Nd	60	13.4371 ± .0071	13.4131 ± .00718	13.4243 ± .0047	12.1456 ± .0047
Sm	62	14.0387 ± .0073	14.0039 ± .0074	13.6837 ± .0049	12.7027 ± .0049
Gd	64	14.6997 ± .00783	14.6639 ± .00783	14.3800 ± .008	13.2463 ± .0082
Hg	80	20.9815 ± .0033	20.8194 ± .0033	19.8824 ± .0033	18.3211 ± .0033
Pb	82	22.0158 ± .0034	21.8025 ± .0033	21.1558 ± .0033	19.1606 ± .0033

and incoherent), pair production cross section according to the theoretical calculation of Tseng and Pratt are shown separately along with the experimental results in Table 4.4.

4.7 Extraction of pair production cross section from the measured total cross section.

Extraction of pair production cross section from the measured total cross section requires the exact knowledge of the competing interactions viz, coherent, incoherent and photoelectric cross section. Coherent and incoherent and cross section are very well known theoretically but unfortunately accurate theoretical calculation for photoelectric effect was not available before 1967. But, after that time a good number of theoretical calculations for photoelectric cross section are available (Ra-67, Sc-67, Sc-73).

This results have been obtained using relativistic calculations which included the effects of screening of the nuclear charge by the atomic electron which are treated relativistically. Rakavy and Ron (Ra-67) calculated cross sections for Z-12, 26, 50, 74 and 92 in the energy range 1-2000 Kev. Schmickley and Pratt (Sc-67) covered 14 elements between z = 13 and 92 in the energy

range 10-3000 Kev Scofield (Sc-73) has calculated cross sections to an accuracy of 1 to 3% for all elements between Z = 1 to 101 in the energy range 1 to 1500 Kev. In view of these theoretical calculations it is now possible to extract the pair production cross section to a better degree of accuracy than was possible previously. For the purpose of extraction of pair production cross section it was necessary to compute the contribution of other competing interaction processes, viz. atomic photoionization cross section, and incoherent and coherent scattering of photons. The cross section of these processes have been computed using the following calculations.

(i) Theoretical atomic photoionization cross sections in the range (1-1.5) Mev from Scofield (Sc-73), in (1.5 -3) Mev from Schimickley and Pratt (Sc-67) and in 3-5 Mev from compilation of Hubbell (Hu-69).

(ii) Hartee-Fock atomic incoherent and coherent scattering factors of Crommer and Mann (Cr-68) as compiled by Hubbell et al (Hu-75).

The main point to be made is presented in fig. 4.2-4.4 where total cross section results from attenuation measurements are displayed together with theoretical

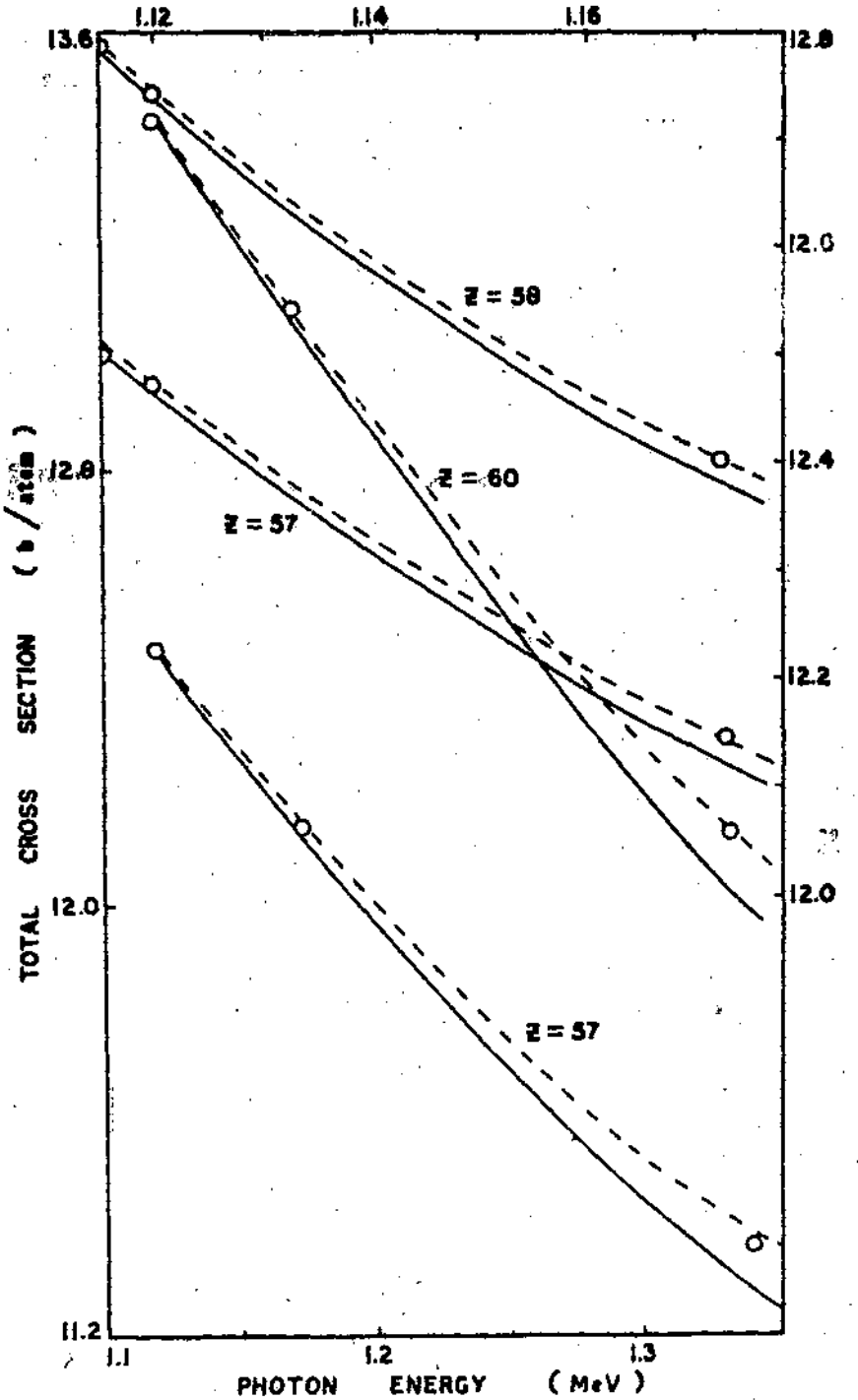

FIG. 4.2. MEASURED TOTAL CROSS SECTION FOR LANTHANUM CERIUM AND NEODOBIAM. (— — —) (COH + INCOH + PHOTO + PAIR CROSS SECTION) (——)(COH + INCOH + PHOTO CROSS SECTION).

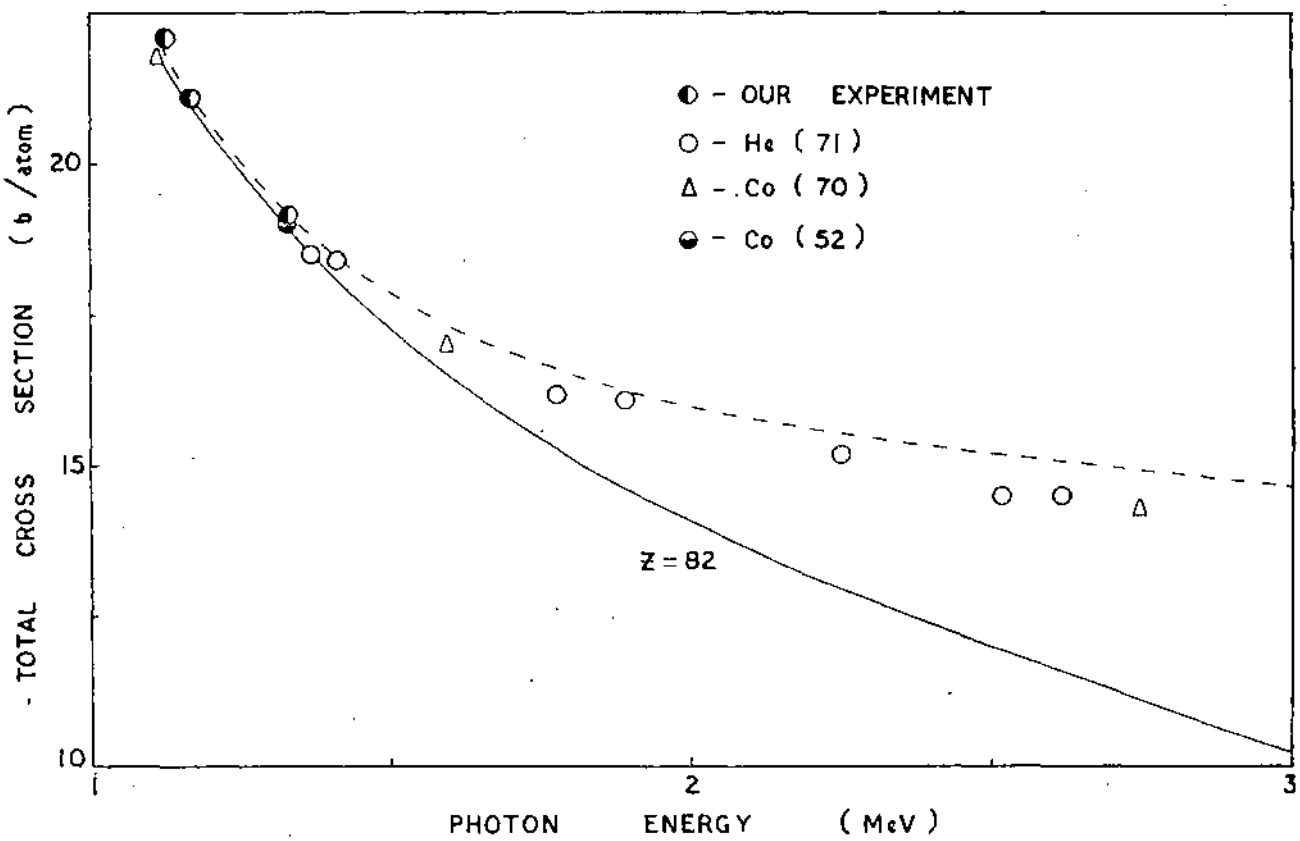

FIG. 4.3. MEASURED TOTAL CROSS SECTION ALONG WITH RESULTS OF SOME OTHER MEASUREMENTS FOR Ph. THEORETICAL CURVE - - - - (COH + INCOH + PHOTO + PAIR PRODUCTION) CROSS SECTION, CURVE ——— THEORETICAL (COH + INCOH + PHOTO) CROSS SECTION.

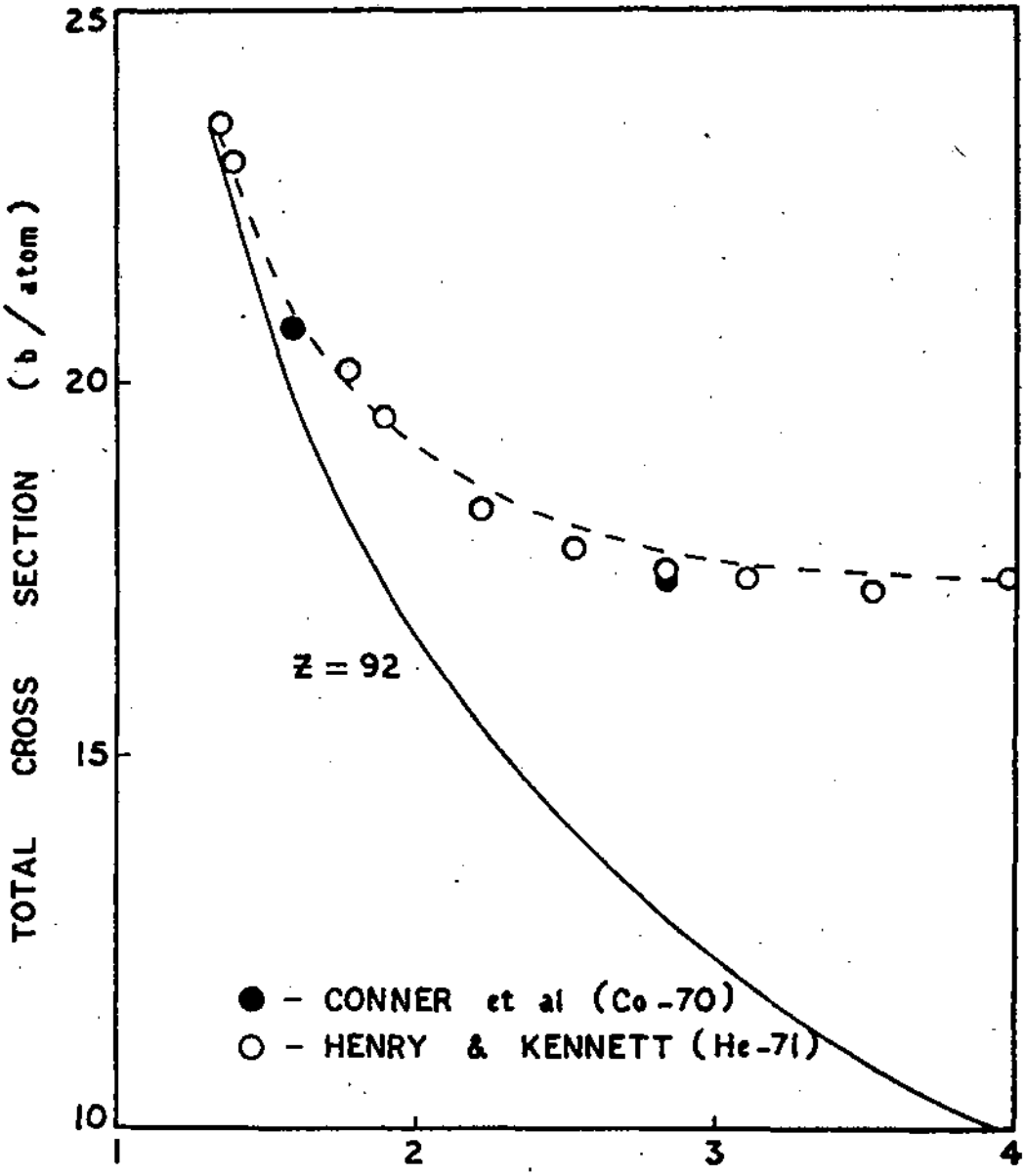

FIG. 4.4. SAME AS IN FIG. 4.3 BUT FOR URANIUM.

curves for the combined interaction processes involved. Theoretical curves of various processes are shown as a function of photon energy in two ways. (a) combined contributions of atomic photoionization, incoherent and coherent scattering of photons (b) atomic pair production, triplet production, photoionization, coherent and incoherent scattering of photons. Such presentation has been given for five elements (Z-57,58,60, 82 and 92).

Theoretical calculation of Tseng and Pratt for the atomic pair production cross section has been used for the evaluation of total cross section in addition to the theoretical calculations of other competing interactions as mentioned earlier. Above a photon energy of 2 Mev the cross section for triplet production according to the calculation as summarized by Hubbell (Hu-69) was taken into account for evaluation of theoretical total cross section.

Fig. 4.2 shows the measured total cross sections for Lanthanum, Cerium and Neodymium along with theoretical cross sections as mentioned. Fig. 4.3 represents the same thing for lead along with the results of other measurements. Fig. 4.4 is for Uranium.

Table - 4.4

Measured total cross section and the theoretical cross section for the competing interactions.

Energy in Mev	Atomic number	Scattering cross section (Coh incoh) in barns/atom	Photoelectric cross section in barns/atom	Pair production cross section in barns/atom	Total a+ b+ c in barns/atom	Measured total cross section in barns/atom
		a	b	c		
	42	8.5042	.2408	.003	8.7480	8.7422 ± .0047
	57	11.5502	.9510	.005	12.5062	12.5072 ± .0069
	58	11.7999	.9858	.005	12.7907	12.7839 ± .006
	60	12.2666	1.2245	.0051	13.4962	13.4371 ± .007
1.115	62	12.6149	1.4199	.006	14.0408	14.0387 ± .007
	64	13.1450	1.5398	.006	14.6858	14.6997 ± .007
	80	16.597	4.4841	.008	21.0891	20.9815 ± .0033
	82	17.0376	4.9646	.009	22.0112	22.0158 ± .0034

Contd..

Table - 4.4 (Contd..)

Energy in Mev	Atomic number	Scattering cross section (Coh incoh) in barns/atom a	Photoelectric cross section in barns/atom b	Pair production cross section in barns/atom c	Total a+b+c in barns/atom	Measured total cross section in barns/atom
	42	8.4844	.2396	.003	8.7270	8.7280 ± .0047
	57	11.5711	.9004	.005	12.4765	12.4769 ± .0069
	58	11.7702	.9740	.005	12.7492	12.7531 ± .006
1.12	60	12.2375	1.21	.0069	13.4544	13.4133 ± .006
	62	12.6021	1.4074	.0069	14.0164	14.0040 ± .0074
	64	13.1137	1.5069	.007	14.6276	14.6639 ± .0078
	80	16.5566	4.172	.008	20.7366	20.8190 ± .0033
	82	16.9955	4.9338	.008	21.9373	21.8045 ± .0034

Contd ...

Table - 4.4 (Contd..)

Energy in Mev	Atomic number	Scattering cross section (Coh incoh) in barns/atom	Photoelectric cross section in barns/atom	Pair production cross section in barns/atom	Total a+b+c in barns atom	Measured total cross section in barns/atom
		a	b	c		
	42	8.2962	.2202	.0082	8.5244	8.5243 ±.0047
	57	11.3431	.8005	.0170	12.1619	12.1629 ±.0069
1.173	58	11.54	.8661	.0177	12.4238	12.4243 ±.0046
	60	11.9564	1.1150	.0193	13.0907	13.0886 ±.0047
	62	12.3726	1.2926	.0210	13.6859	13.6837 ±.005
	64	12.8702	1.4074	.0227	14.3845	14.3800 ±.007
	80	16.1174	3.7281	.0384	19.8889	19.882 ±.003
	82	16.6234	4.5003	.0405	21.1690	21.1558 ±.003

Contd..

Table - 4.4 (Contd..)

Energy in Mev	Atomic number	Scattering cross section (Coh incoh) in barns/atom	Photoelectric cross section in barns/atom	Pair production cross section in barns/atom	Total a+b+c in barns/atom	Measured total cross section in barns/atom
		a	b	c		
	42	7.7640	.1730	.041	7.9780	7.9788 ± .003
	57	10.6005	.6796	.0897	11.3698	11.3699 ± .0046
	58	10.7401	.7499	.0969	12.5869	11.6100 ± .008
1.332	60	11.1637	.8739	.106	12.1436	12.1456 ± .0047
	62	11.5468	1.0132	.116	12.6860	12.6909 ± .005
	64	11.9308	1.1691	.136	13.2359	13.2462 ± .005
	80	14.8836	3.1973	.244	18.3249	18.3211 ± .003
	82	15.4016	3.51	.254	19.1656	19.1606 ± .0033

From the figures 4.2 - 4.4 it is seen that total cross section measurement experiments are adequately suitable for infering unambiguous conclusion on pair production theory in the threshold region. The extracted pair production cross section is shown in Table 4.5.

In view of the development in the theoretical calculations of photoelectric cross section, it seems reasonable to reanalyse the total cross section measurement data for the evaluation of pair production cross section. For the purpose of reanalysis we have selected the total cross section measurement data of Henry and Kennett (He-71) and Conner et al (Co-70). Pair production cross section as evaluated after reanalysis of these data are given in Table 4.6 along with the measured pair production cross section of Henry and Kennett and the recent theoretical calculations of atomic pair production cross sections at nine different energies.

Table - 4.5

Extracted pair production cross section from the measured total cross section along with theoretical results. σ_B-Born approximation results (unscreened) $\sigma_{pc}^{\phi o}$ Øverbo point coulomb calculation $\sigma_{sc}^{\phi o}$ Øverbo screening corrected calculation σ_{sc}^{TP}-Tseng and Pratt screening corrected calculations in b/atom.

Energy in Mev	Target Z	σ_B in barns per atom	$\sigma_{Pc}^{\phi o}$ in barns per atom	$\sigma_{Sc}^{\phi o}$ in barn per atom	σ_{Sc}^{TP} in barns per atom	Experimental results in barns per atom
	42	4.75×10^{-3}	7.67×10^{-3}	8.24×10^{-3}	7.67×10^{-3}	$7.9\times10^{-3}\pm.004$ - 2
	57	8.76×10^{-3}	1.59×10^{-2}	1.83×10^{-2}	1.7×10^{-2}	$1.64\times10^{-2}\pm.0069$
	58	9.07×10^{-3}	1.66×10^{-2}	1.9×10^{-2}	1.77×10^{-2}	$1.73\times10^{-2}\pm.007$
1.173	60	9.7×10^{-3}	1.79×10^{-2}	2.09×10^{-2}	1.93×10^{-2}	$1.74\times10^{-2}\pm.007$
	62	1.03×10^{-2}	1.91×10^{-2}		2.1×10^{-2}	$2.07\times10^{-2}\pm.007$
	64	1.1×10^{-2}	2.06×10^{-2}		2.27×10^{-2}	$2.26\times10^{-2}\pm.007$
	80	1.72×10^{-2}	3.2×10^{-2}	4.32×10^{-2}	3.84×10^{-2}	$4.05\times10^{-2}\pm.003$
	82	1.81×10^{-2}	3.35×10^{-2}	4.53×10^{-2}	4.05×10^{-2}	$4.32\times10^{-2}\pm.003$

Contd..

Table - 4.5 (Contd..)

Energy in Mev	Target Z	σ_β in barns per atom	$\sigma^{\phi o}_{Pc}$ in barns per atom	$\sigma^{\phi o}_{Sc}$ in barns per atom	σ^{TP}_{Sc} in barns per atom	Experimental results in barns per atom
	42	2.85×10^{-2}	4.04×10^{-2}	4.14×10^{-2}	4.1×10^{-2}	$4.1\times10^{-2}\pm .003$
	57	5.26×10^{-2}	8.94×10^{-2}	9.35×10^{-2}	9.24×10^{-2}	$8.97\times10^{-2}\pm .004$
	58	5.44×10^{-2}	9.35×10^{-2}	9.81×10^{-2}	9.69×10^{-2}	$9.65\times10^{-2}\pm .004$
1.332	60	5.83×10^{-2}	1.026×10^{-1}	1.08×10^{-1}	1.065×10^{-1}	$1.06\times10^{-1}\pm .004$
	62	6.22×10^{-2}	1.119×10^{-1}		1.16×10^{-1}	$1.42\times10^{-1}\pm .005$
	64	6.03×10^{-2}	1.219×10^{-1}		1.27×10^{-1}	$1.36\times10^{-1}\pm .005$
	80	1.036×10^{-1}	2.214×10^{-1}	2.44×10^{-1}	2.27×10^{-1}	$2.38\times10^{-1}\pm .003$
	82	1.089×10^{-1}	2.359×10^{-1}	2.63×10^{-1}	2.54×10^{-1}	$2.49\times10^{-1}\pm .003$

Table - 4.6

Experimental results of Henry and Kennett, renalysed results of their data along with theoretical calculations. σ_B B-Born approximation results, $\sigma_{Pc}^{\phi o}$ - point coulomb calculation of ϕverbo, $\sigma_{Sc}^{\phi o}$ - screening corrected calculation of ϕverbo, σ_{Sc}^{TP} - screening corrected calculation of Tseng and Pratt.

Energy in Mev	Atomic number	σ_B in barns per atom	$\sigma_{Pc}^{\phi o}$ in barns per atom	$\sigma_{Sc}^{\phi o}$ in barns per atom	σ_{Sc}^{TP} in barns per atom	Experimental H.K. in barns/atom	Our reanalysis of H.K. data in barns per atom	Our reanalysis of Conner et al in barns per atom
	42	.195			2.33		.253	
1.778	82	.743	1.284	1.311	1.309	.9 ± .3	1.208 ± .3	
	92	.9356	1.75		1.79	1.6 ± .4	2.03 ± .4	
	29	.1194		.129	.129		.1134	
1.888	42	.2506		.292			.274	
	82	.9546	1.565	1.587	1.59	1.4 ± .3	1.71 ± .3	
	92	1.201	2.12		2.16	1.9 ± .4	2.26 ± .4	

Table - 4.6 (Contd..)

Energy in Mev	Atomic number	σ_β in barns per atom	$\sigma_{Pc}^{\phi\phi}$ in barns per atom	$\sigma_{Sc}^{\phi\phi}$ in barns per atom	σ_{Sc}^{TP} in barns per atom	Experimental H.K. in barns/atom	Our reanalysis of H.K. data in barns per atom	Our reanalysis of Conner et al in barns per atom
	29			.220	.220		.256	
	42				.483		.443	
2.225	92		3.20		3.26	2.7 .3	3.11 .3	
	29	.355			.370		.377	.378
2,754	42	.745			.798		.750	.84
	82	2.839	3.614	3.607	3.63	3.1±.3	3.12±.3	3.21
	92	3.5746	4.69		4.73	4.2±.3	4.16±.3	4.41

Contd..

Table - 4.6 (Contd..)

Energy in Mev	Atomic number	σ_β in barns per atom	$\sigma_{Pc}^{\phi\phi}$ in barns per atom	$\sigma_{Sc}^{\phi\phi}$ in barns per atom	σ_{Sc}^{TP} in barns per atom	Experimental H.K. in barns/atom	Our reanalysis of H.K. data in barns per atom	Our reanalysis of Conner et al in barns per atom
	29	.451		4.76	.465		.472	
3.098	42	.947			.996		.951	
	82	3.60	4.32	4.30	4.33	4.00 ± .2	4.11 ± .2	
	92	4.538	5.55			5.3 ± .2	5.49 ± .2	
	29	.568		.580	.574		.63	
	42	1.19			1.238		1.237	
3.53	82	4.54	5.14	5.15	5.15	4.7 ± .2	4.75 ± .2	
	92	5.71	6.53			6.2 ± .3	6.328 ± .3	

Contd..

Table - 4.6 (Contd..)

Energy in Mev	Atomic number	σ_B in barns per atom	$\sigma_{Pc}^{\phi\phi}$ in barns per atom	$\sigma_{Sc}^{\phi\phi}$ in barns per atom	σ_{Sc}^{TP} in barns per atom	Experimental H.K. in barns/atom	Our reanalysis of H.K. data in barns per atom	Our reanalysis of Conner et al in barns per atom
	29	.606		.611	.618		.629	
3.675	42	1.272			1.50		1.289	
	82	4.845	5.40	5.42	5.41	5.1±.2	5.12±.2	
	92	6.098	6.85			6.5±.2	6.65±.2	
	42				1.5015		1.454	
3.985	82		5.94	5.949	5.958	5.5±.2	5.54±.2	
	92		7.48			7.3±.2	7.48±.2	
	29	.8134			.8153		.82	
4.508	42	1.706			1.8069		1.75	
	82	6.50	6.78	6.753	6.78	6.4±.2	6.45±.2	
	92	8.186	8.49			8.1±.3	8.34±.3	

4.6 DISCUSSION

For the purpose of comparison with the theoretical calculation of pair production cross section the theoretical cross sections have been plotted against energy for few elements along with experimental results.

In Fig. 4.5 pair production cross section according to the theoretical calculation of Øverbo (point coulomb) and screening corrected calculation of Tseng and Pratt has been displayed for Z = 42, 60 and 80 along with our experimental results and results of direct measurement of Henry and Kennett (He-72). In Fig. 4.6 the present experimental results, the results of direct measurement of Henry and Kennett are shown for Pb along with theoretical calculations of Øverbo (Point) Coulomb) and screening corrected calculation of Tseng and Pratt. In Fig. 4.7 theoretical cross section according to the calculation of Tseng and Pratt are displayed for Copper, Molybdenum and lead and Uranium.

Pair production cross section as evaluated by Henry and Kennett (He-71) from total cross section measurement are shown in Fig. 4.7. The evaluated pair production cross section from reanalysis of the data of Henry and Kennett, and of Conner et al are also shown in the same fig. In all cases results of the present reanalysis show better agreement with screening corrected pair production cross section of

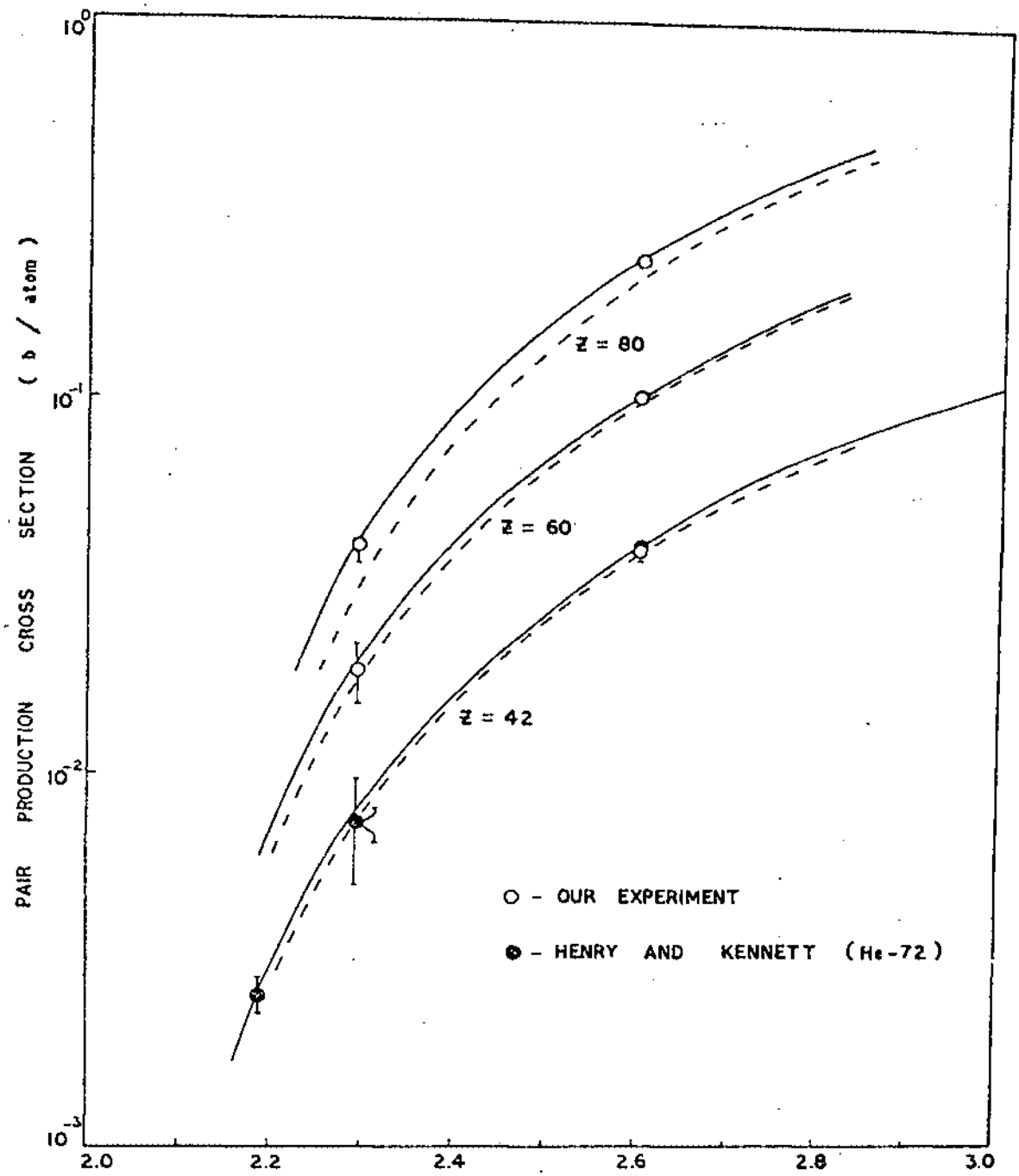

FIG. 4.5. PAIR PRODUCTION CROSS SECTION VS ENERGY FOR Z = 42, 60 AND 80. CURVE – – – (Øo -67) ——— (Ts -72)

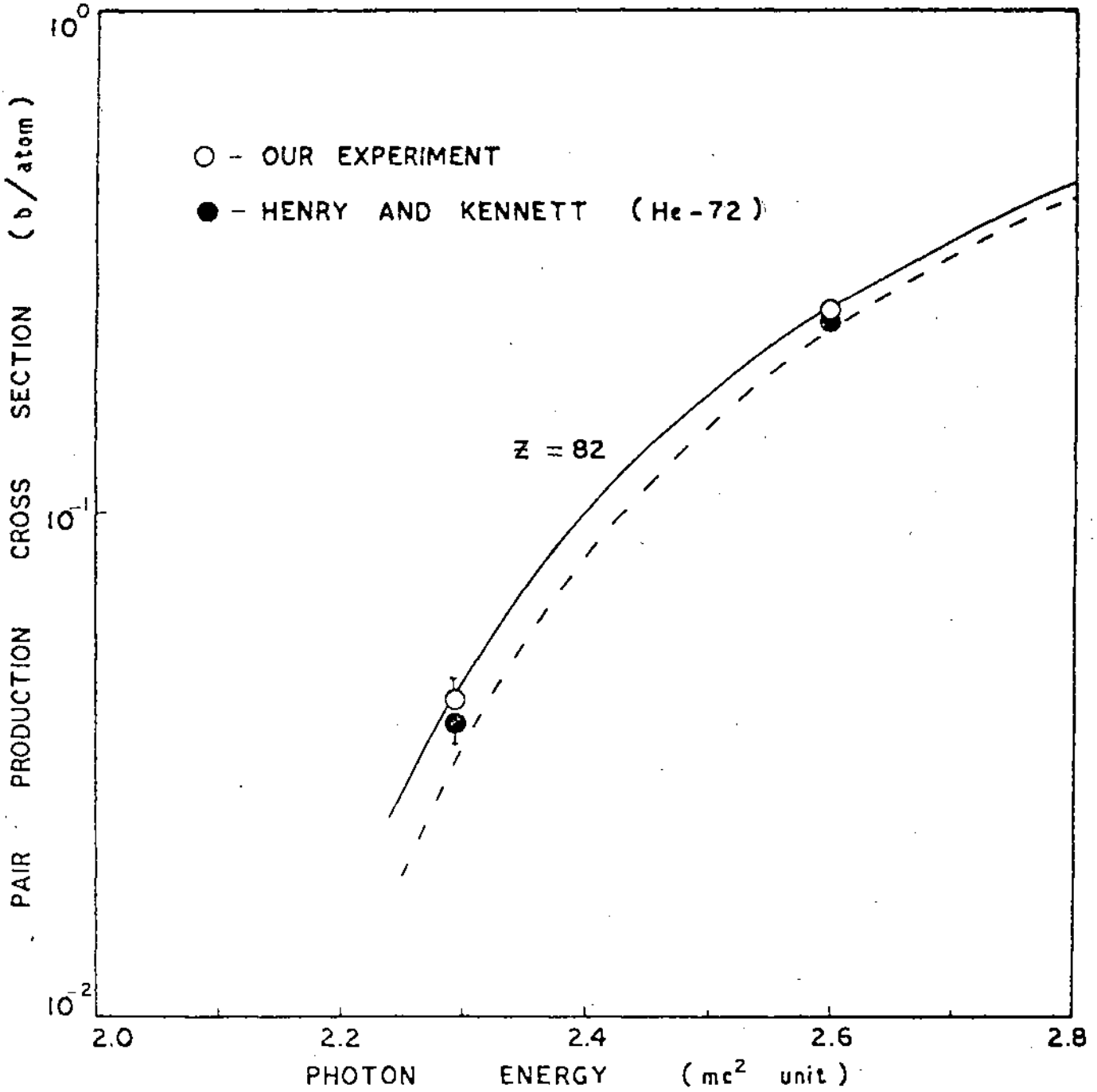

FIG. 4.6. SAME AS IN FIG. 4.5 BUT FOR LEAD.

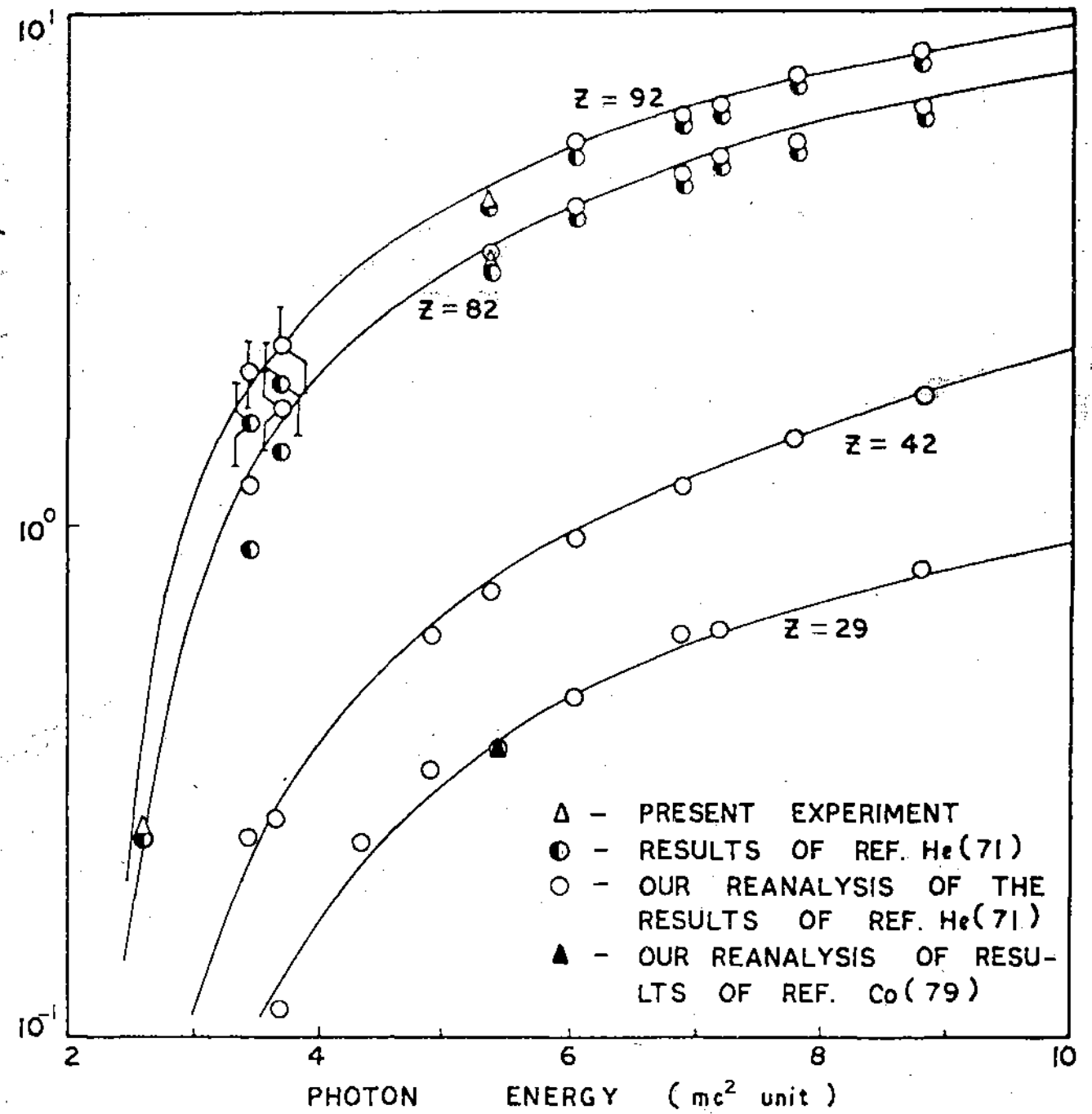

FIG. 4.7. PAIR PRODUCTION CROSS SECTION VS ENERGY FOR Z = 29, 42, 82 AND 92. CURVE – PAIR PRODUCTION CROSS SECTION ACCORDING TO REF. Ts(72).

Tseng and Pratt.

Since pair production cross section varies by several order of magnitude with change in energy it is convenient to base the presentation of the measured pair production cross section in terms of Born approximation pair production cross section.

Pair production cross section relative to Born approximation results according to different theoretical calculations are shown in Fig. 4.8-4.12 as a function of atomic number at different energies. In Fig. 4.8 σ/σ_B at 1.119 Mev has been plotted against atomic number. The results of direct measurement of pair production cross section of Girard et al (Av -74) and Rao et al (Ra-63) are also shown. In Fig. 4.9 the ratio σ/σ_B has been plotted against atomic number at 1.173 Mev. The present experimental results and the results of direct measurement of Henry and Kennett are also shown.

In Fig. 4.10 σ/σ_B with atomic number has been shown for 1.332 Mev and 2.615 Mev along with the present experimental results, the results of direct measurements of Henry and Kennett, Dayton (Da-52). Girard et al are shown. At 2.615 Mev reanalysed results of Colgate's data are also shown.

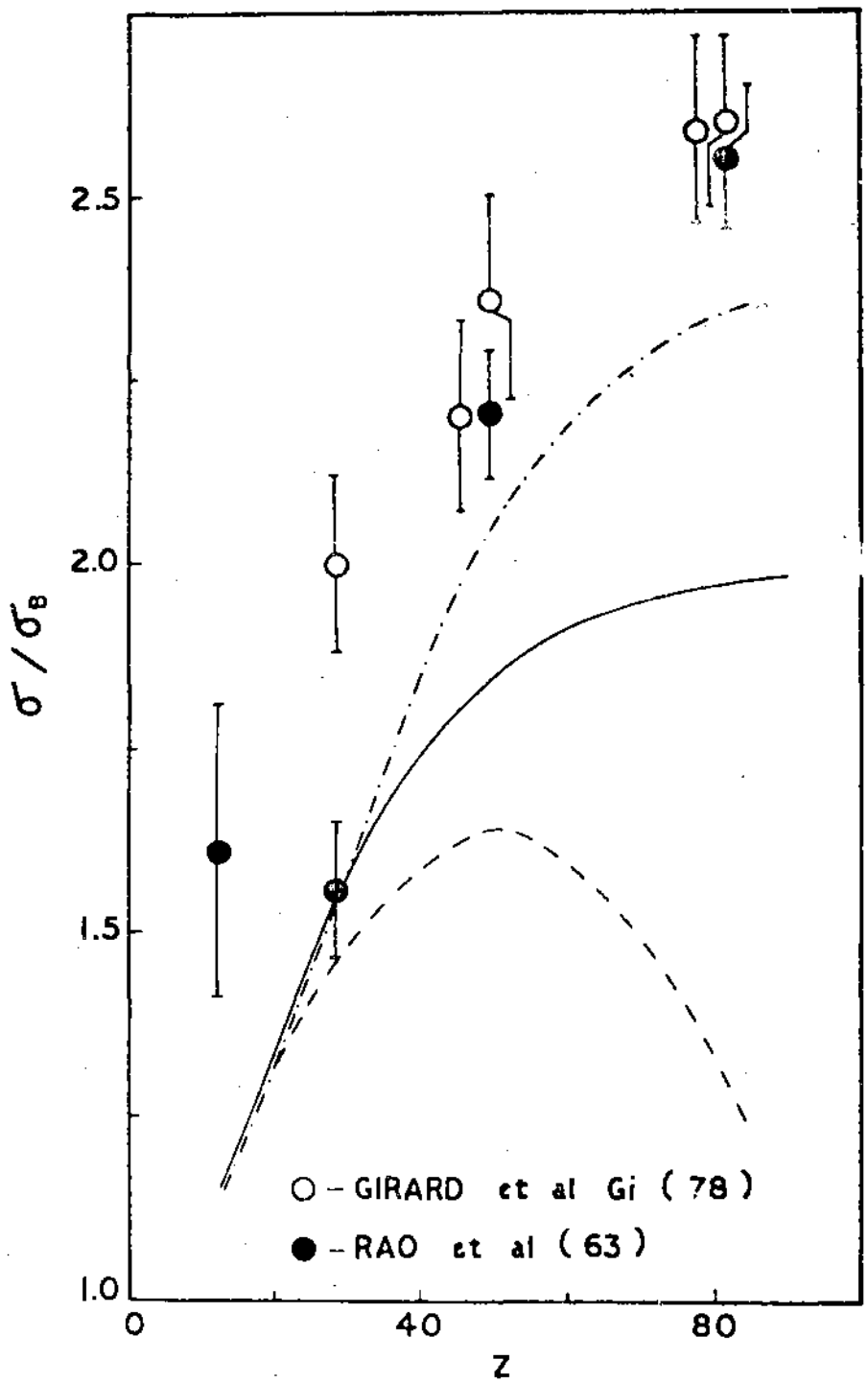

FIG. 4.8. σ / σ_B VS Z AT 1.119 MeV. CURVE – – – Øo (67) ——— Ts (72) –·–·– Øo (79)

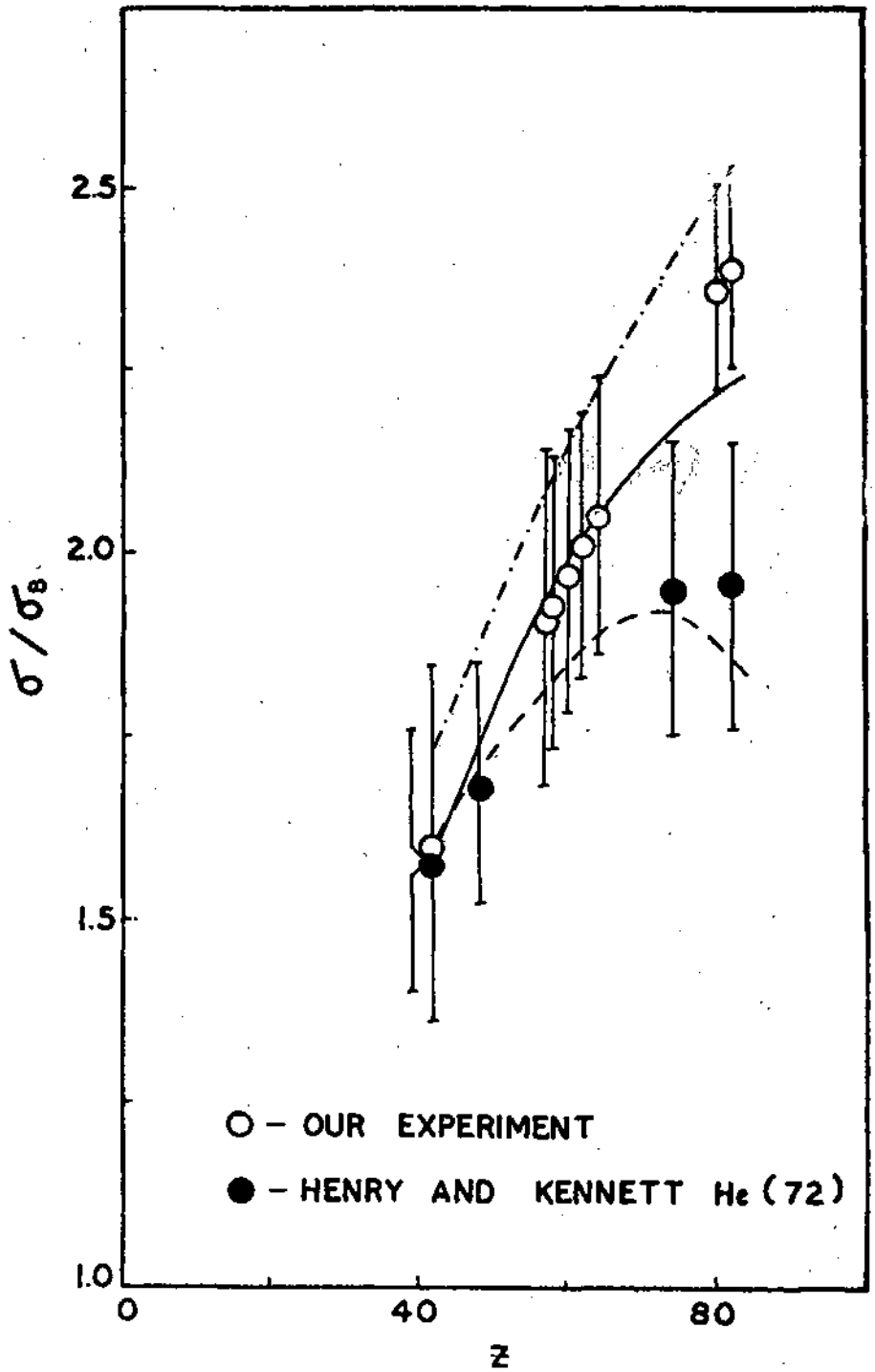

FIG. 4.9. SAME AS IN FIG. 4.8 BUT AT 1.173 MeV.

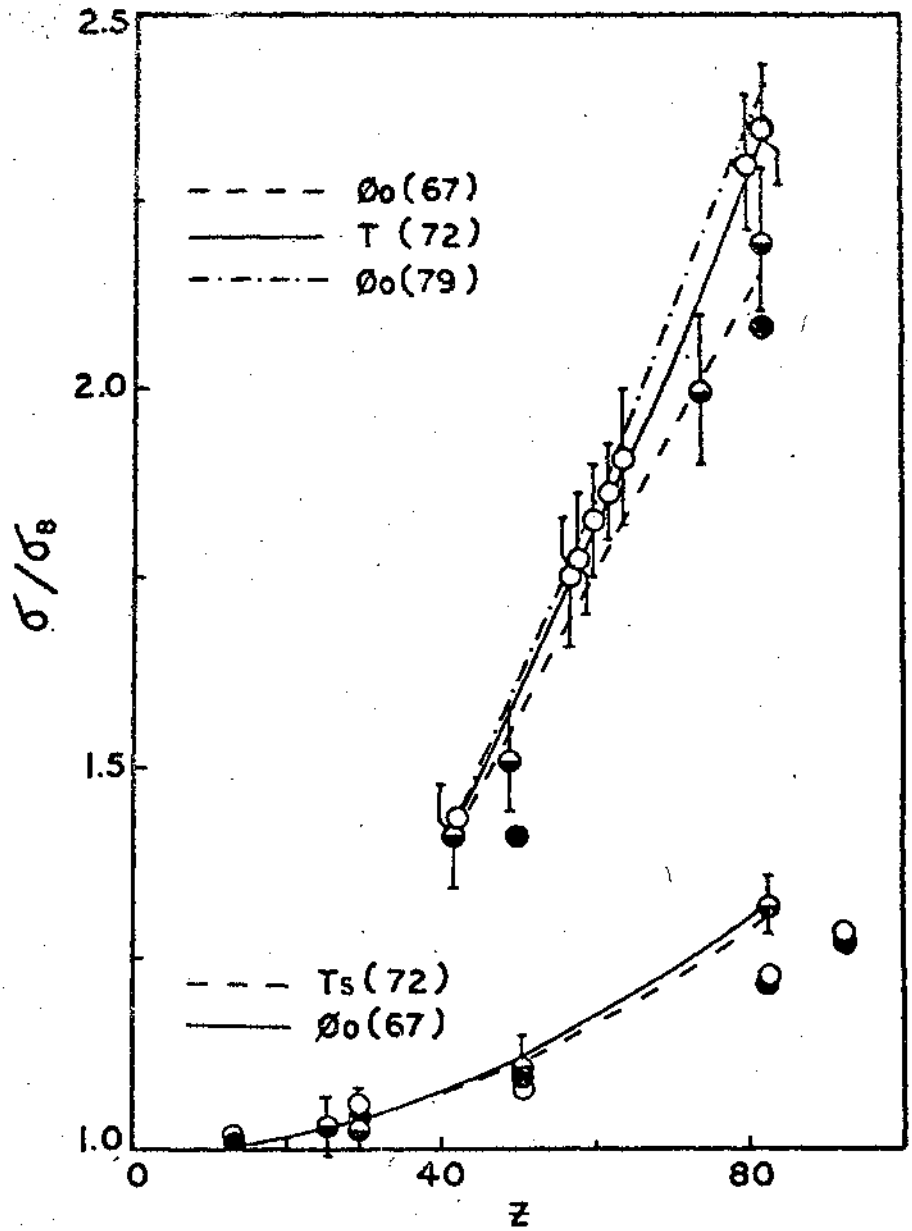

FIG. 4.10. SAME AS IN FIG. 4.8 BUT AT 1.332 MeV (UPPER) & 2.615 MeV (LOWER). POINTS AT 1.332 ○ - OUR EXPERIMENT, ◒ - REF. He (72), ● - REF. Da (53) AND POINTS AT 2.615 ◒ - REF. Gi (78), ○ - REF. Da (53), ◉ - OUR REANALYSIS OF THE DATA OF REF. Co (50).

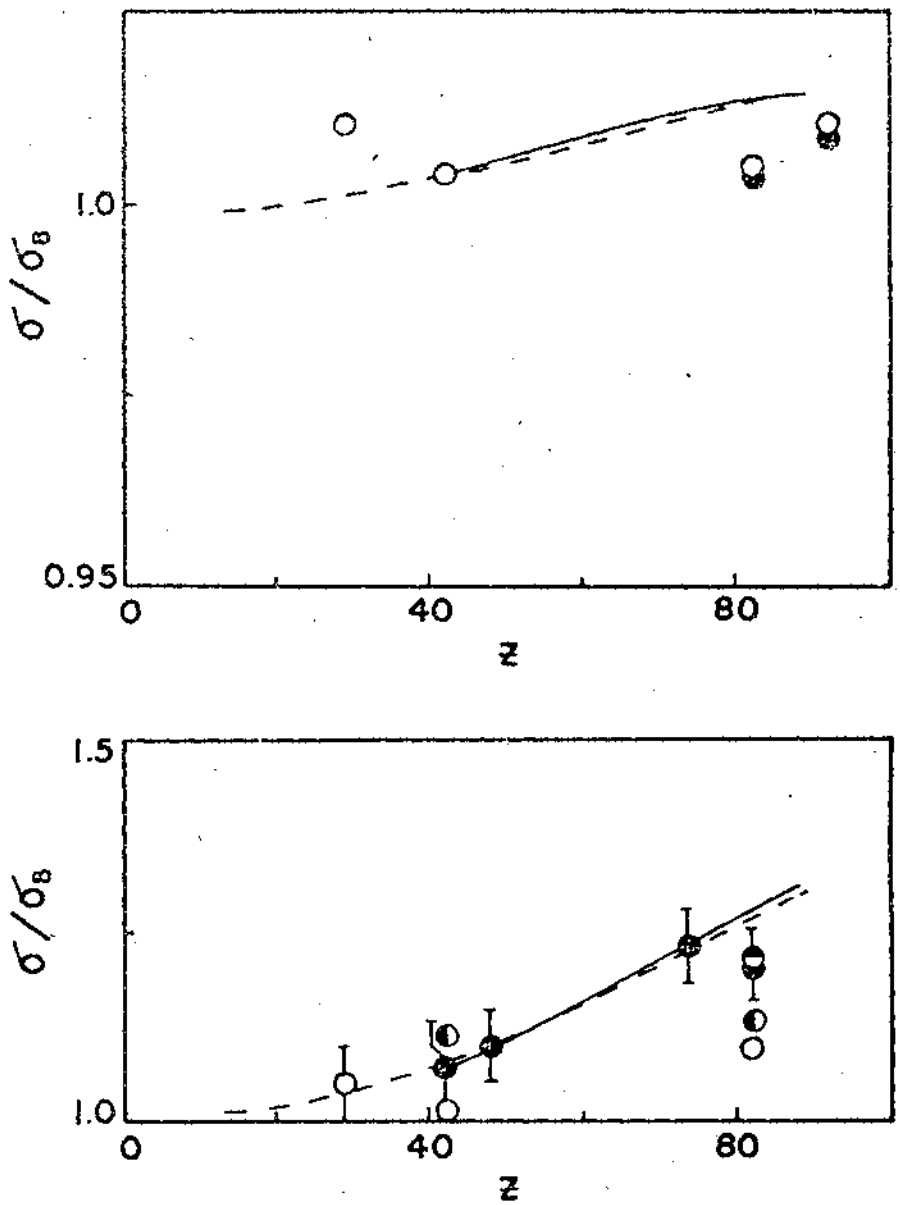

FIG. 4.11. SAME AS IN FIG. 4.8 BUT AT 3.53 MeV (UPPER) AND 2.754 MeV (LOWER). CURVES —— Ts(72) – – – Øo(67). POINTS (UPPER) ◍ - REF. He(71), ○ – OUR RE-ANALYSIS OF THE DATA OF REF. He(71), POINTS (LOWER) ◍ - REF. He(71), ○ - OUR RE-ANALYSIS OF THE DATA OF REF. He(71), ◐ – OUR REANALYSIS OF THE DATA OF REF. Co(70) AND ◓ - REF. St(58).

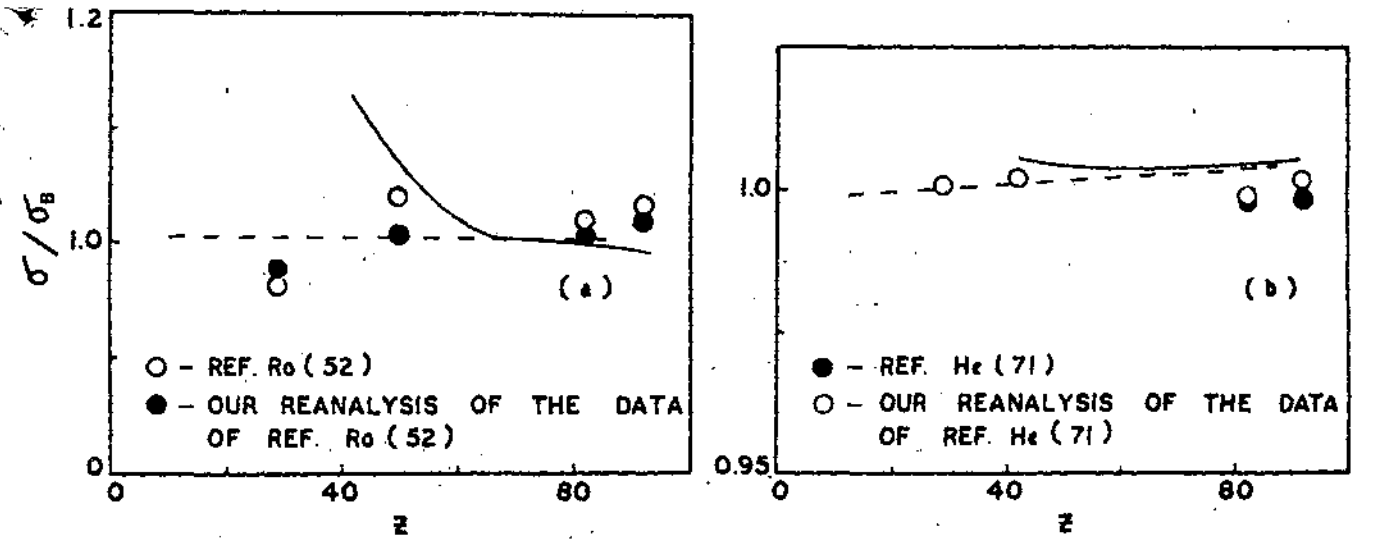

FIG. 4.12 a and b. SAME AS IN FIG. 4.8 BUT AT 5.3 MeV (a) AND 4.5 MeV (b). CURVE – – – REF. Øo (67) AND ——— REF. Ts (72)

Fig. 4.11 shows σ/σ_β at 3.53 Mev and 2.754 Mev according to point Coulomb calculation of Øverbo and screening corrected calculation of Tseng and Pratt against atomic number. At 3.53 Mev Experimental results of Henry and Kennett and reanalysed results of their data are also shown.

At 2.754 Mev experimental results of Henry and Kennett, Standil and Shkolnik (St-58), reanalysed results of the data Henry and Kennett, Conner et al are shown.

In Fig. 4.12 σ/σ_β at 5.3 Mev and 4.50 Mev are shown according to the calculation of Tseng and Pratt and Point Coulomb Calculation of Øverbo.

At 5.3 Mev experimental results of Rosenblum et al (Ro-52), reanalysed results of Rosenblum's data are shown.

At 4.50 Mev Experimental results of Henry and Kennett and reanalysed results of their data has been displayed.

From Fig. 4.8 it is evident that error bars to the experimental results of Girard et al do not touch the theoretical calculation of Øverbo (Øo-79) who has taken screening of the atomic electrons into account at 1.119 Mev except for Z = 29. Experimental results of Rao et al (Ra-63) are also not in agreement with theoretical ratio. In Fig. 4.9 for medium Z elements the presently evaluated cross section results from total cross section measurement show

excellent agreement with the screening corrected calculation of Tseng and Pratt. At high Z (80,82) however there is a trend in support of the screening corrected calculations of Øverbo (Øo-79). At 1.332 Mev the presently evaluated cross sections are in very good agreement with calculations of Tseng and Pratt whereas the experimental results of Dayton (Da-52) shows no definite trend (Fig. 4.10). Experimental points of Henry and Kennett however show a trend of agreement with point coulomb calculations of Øverbo. At 2.615 Mev the screening corrections become negligible for low Z elements. The experimental results of Girard et al are in good agreement with calculations of Tseng and Pratt. Again experimental points of Dayton (Da-52) are well below the theoretical ratio. The reanalysed data of Henry and Kennett are in better agreement with recent theoretical calculations at 3.53 Mev and 2.754 Mev (Fig. 4.11). Also at 5.3 Mev and 4.5 Mev the results after reanalysis is found to agree better with the theoretical calculation of Tseng and Pratt (Fig. 4.12).

It will not be out of place to mention some of the recent total cross section measurement experiments for extraction of photo electric cross section by subtraction method.

Shiva Sankar Rao et al (Si-76) made measurements on a number of elements below 1 Mev and extracted results

were in good agreement with calculations of Scofield (Sc-73).

In the energy range between 3.3 to 165.8 Kev total cross section experiments were carried out by Parthasaradhi et al (Pa-74).

Ramkrishna Gowda et al (Ra-76), V.Lakshiminarayana et al (La-82), Sanjeevaiah et al (Sa-82) have also made attenuation measurements for the ectraction of photo electric cross section and in all cases agreement with theoretical calculations of Scofield are reasonably good.

The present measurement and analysis therefore show unambiguously the suitability of total cross section measurement for extraction of atomic pair production cross section at energies near threshold (i.e. 1.173, 1.332). In the energy region near threshold where disagreement between direct measurements and theoretical prediction is the greatest (Fig. 4.8) . Our measurements indicate unity with theory, although the method is not sensitive enough at these low energies to distinguish between the results of Øverbo and Tseng and Pratt. At higher energies however since most accurate theoretical calculations of photoelectric cross sections (Sc-73) are now available the total cross section measurement to extract pair production cross section deserves more attention.